2008

Overexpression of ABCA1 reduces amyloid deposition in the PDAPP mouse model of Alzheimer disease

Suzanne E. Wahrle
Washington University School of Medicine in St. Louis

Hong Jiang
Washington University School of Medicine in St. Louis

Maia Pasandanian
Washington University School of Medicine in St. Louis

Jungsu Kim
Washington University School of Medicine in St. Louis

Aimin Li
Washington University School of Medicine in St. Louis

See next page for additional authors

Overexpression of ABCA1 reduces amyloid deposition in the PDAPP mouse model of Alzheimer disease

Suzanne E. Wahrle,[1] Hong Jiang,[1] Maia Parsadanian,[1] Jungsu Kim,[1] Aimin Li,[2] Amanda Knoten,[3] Sanjay Jain,[3] Veronica Hirsch-Reinshagen,[4] Cheryl L. Wellington,[4] Kelly R. Bales,[5] Steven M. Paul,[5] and David M. Holtzman[1,6,7,8]

[1]Department of Neurology, [2]Department of Cell Biology and Physiology, [3]John T. Milliken Department of Medicine, Renal Division, Washington University School of Medicine, St. Louis, Missouri, USA. [4]Department of Pathology and Laboratory Medicine, University of British Columbia, Vancouver, British Columbia, Canada. [5]Neuroscience Discovery Research, Eli Lilly and Company, Lilly Research Laboratories, Indianapolis, Indiana, USA. [6]Edward Mallinckrodt Department of Developmental Biology, [7]Hope Center for Neurological Disorders, and [8]Alzheimer's Disease Research Center, Washington University School of Medicine, St. Louis, Missouri, USA.

***APOE* genotype is a major genetic risk factor for late-onset Alzheimer disease (AD). ABCA1, a member of the ATP-binding cassette family of active transporters, lipidates apoE in the CNS. *Abca1*$^{-/-}$ mice have decreased lipid associated with apoE and increased amyloid deposition in several AD mouse models. We hypothesized that mice overexpressing ABCA1 in the brain would have increased lipidation of apoE-containing lipoproteins and decreased amyloid deposition. To address these hypotheses, we created *PrP-mAbca1* Tg mice that overexpress mouse *Abca1* throughout the brain under the control of the mouse prion promoter. We bred the *PrP-mAbca1* mice to the PDAPP AD mouse model, a transgenic line overexpressing a mutant human amyloid precursor protein. PDAPP/*Abca1* Tg mice developed a phenotype remarkably similar to that seen in PDAPP/*Apoe*$^{-/-}$ mice: there was significantly less amyloid β-peptide (Aβ) deposition, a redistribution of Aβ to the hilus of the dentate gyrus in the hippocampus, and an almost complete absence of thioflavine S–positive amyloid plaques. Analyses of CSF from *PrP-mAbca1* Tg mice and media conditioned by *PrP-mAbca1* Tg primary astrocytes demonstrated increased lipidation of apoE-containing particles. These data support the conclusions that increased ABCA1-mediated lipidation of apoE in the CNS can reduce amyloid burden and that increasing ABCA1 function may have a therapeutic effect on AD.**

Introduction

ABCA1, a member of the ATP-binding cassette family of active transporters, mediates the rate-limiting step of the reverse cholesterol transport pathway, which eliminates excess cellular cholesterol and protects against atherosclerosis (1–5). Specifically, ABCA1 transfers cellular cholesterol and phospholipids onto lipid-poor apolipoproteins to form pre-β HDL particles in the plasma. These pre-β HDL lipoprotein particles undergo subsequent cholesterol esterification and mature into spherical HDL particles that shuttle cholesterol to the liver for excretion as bile acids. Loss-of-function mutations in ABCA1 cause Tangier disease, which is characterized by very low levels of HDL cholesterol and apoA-I in plasma, accumulation of cholesterol in lymphatic organs, and an increased risk of cardiovascular disease (6–12). The low levels of apoA-I result from increased degradation of lipid-poor apoA-I (13, 14). In animal models, upregulation of ABCA1 can increase HDL cholesterol and protect against atherosclerosis (15–17).

ABCA1 also has an important role in the CNS. The CNS contains HDL-like lipoprotein particles composed mainly of apoE, cholesterol, and phospholipids. Mice lacking ABCA1 have dramatically lower apoE in the plasma, cerebrospinal fluid (CSF), and brain (18–20), probably because like lipid-poor apoA-I, lipid-poor apoE is rapidly degraded. Interestingly, CSF from *Abca1*$^{-/-}$ mice contains a population of apoE-containing lipoprotein particles that are abnormally small (18). Additionally, nascent apoE-containing lipoprotein particles secreted from primary cultures of astrocytes, the major source of apoE in the CNS, are abnormally small and lipid poor if they are derived from *Abca1*$^{-/-}$ mice (18). These data strongly suggest that ABCA1 is the major molecule that lipidates apoE in the CNS and that the ABCA1 plays as critical a role in apoE lipoprotein metabolism in the brain as it does in apoA-I and HDL metabolism in the periphery.

APOE genotype is the major genetic risk factor for late-onset Alzheimer disease (AD). It is theorized that apoE binds to amyloid β-peptide (Aβ) and influences its clearance and conformation. For example, apoE binding may affect the ratio of Aβ that is in a random coil versus a β-sheet (21). Many mouse models of AD have been created that overexpress mutant human forms of the amyloid precursor protein (APP) and develop AD-like deposits of Aβ in brain. The Aβ in many of these plaques is arranged into fibrils with a high β-pleated sheet content that bind the dyes Congo red and thioflavine S. These fibrillar amyloid plaques are associated with abnormal axons and dendrites (neuritic dystrophy) and a surrounding area of decreased synaptic density (22). We and others have shown that apoE contributes to amyloid burden in vivo, as APP Tg mice that are crossed to mice lacking *Apoe* develop significantly less Aβ deposition, and strikingly, the Aβ plaques that do

Nonstandard abbreviations used: Aβ, amyloid β-peptide; ACM, astrocyte-conditioned media; AD, Alzheimer disease; APP, amyloid precursor protein; CAA, cerebral amyloid angiopathy; CSF, cerebrospinal fluid; LDLR, LDL receptor; LRP1, LDLR-related protein 1.

Conflict of interest: The authors have declared that no conflict of interest exists.

Citation for this article: *J. Clin. Invest.* **118**:671–682 (2008). doi:10.1172/JCI33622.

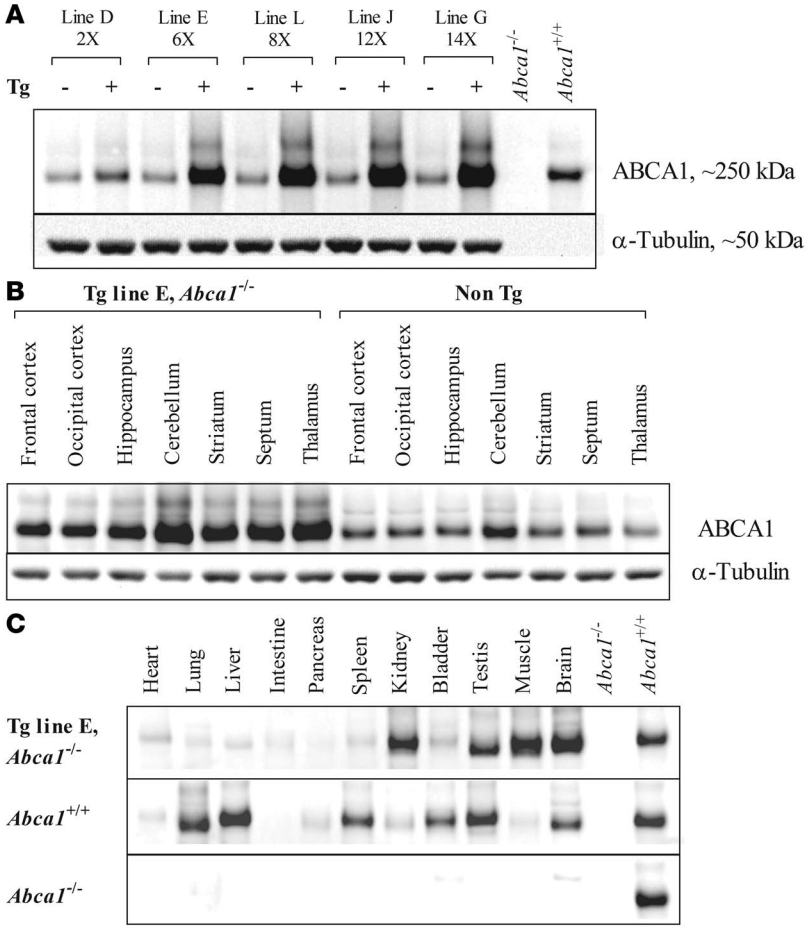

Figure 1

Characterization of 3-month-old *PrP-mAbca1* mice. (**A**) Levels of ABCA1 in the cortex of 5 different lines of *PrP-mAbca1* mice (lines D, E, L, J, and G) were visualized by Western blotting. RIPA lysates were made from cortex, and equal amounts of total protein (10 μg) were electrophoresed. Western blotting of ABCA1 was performed using the HJ1 antibody. Samples from Tg (+) and non-Tg mice (–) were compared. Liver lysates from *Abca1*$^{+/+}$ and *Abca1*$^{-/-}$ mice were used as positive and negative controls, respectively. The fold difference in ABCA1 overexpression was estimated by diluting the Tg sample until the level of ABCA1 equaled that of the non-Tg sample. (**B**) ABCA1 expression in multiple brain regions was assessed by Western blotting in *PrP-mAbca1* line E mice. (**C**) ABCA1 expression in major body tissues was examined in mice expressing no ABCA1 (bottom panel), the *PrP-mAbca1* transgene with no endogenous ABCA1 (the top panel), and endogenous ABCA1 (middle panel). Liver lysates from *Abca1*$^{+/+}$ and *Abca1*$^{-/-}$ mice were used as positive and negative controls, respectively.

form are almost all nonfibrillar and are not associated with neuritic dystrophy (20, 23, 24). Since *Abca1*$^{-/-}$ mice have dramatically lower levels of apoE, it might be expected that crossing them to APP Tg mice would result in a phenotype similar to that of APP/*Apoe*$^{-/-}$ mice. However, 3 laboratories independently found that deletion of *Abca1* either has no effect on or even increases Aβ deposition in 4 different mouse models of AD (20, 23, 24). These results suggest that the poorly lipidated apoE-containing lipoprotein particles produced by *Abca1*$^{-/-}$ mice may increase Aβ deposition and fibrillogenesis. Additionally, apoE codeposited with fibrillar Aβ (23), and *Abca1*$^{-/-}$ mice accumulated insoluble apoE to a greater extent than *Abca1*$^{+/+}$ mice (23, 24), demonstrating that lipid-poor apoE binds to fibrillar Aβ in vivo and likely promotes amyloidogenesis.

Since lipid-poor apoE is associated with increased amyloid deposition in vivo, we hypothesized that increased lipidation of apoE via ABCA1 would lower amyloid deposition. Three transgenic ABCA1 mouse models have been generated previously; 2 that express genomic ABCA1 as a BAC (25, 26) and 1 expressing ABCA1 cDNA under the control of the apoE/C1 locus (27). However, none of these models have appreciable overexpression of ABCA1 in the brain. Moreover, crossing ABCA1 BAC Tg mice to APP/PS1 mice did not result in altered Aβ deposition, likely because brain ABCA1 levels were not significantly increased relative to those in non-Tg APP/PS1 mice (26). Therefore, to create mice with abundant overexpression of ABCA1 in the brain, we cloned the mouse *Abca1* cDNA, inserted it into the MoPrP.HD-N171 transgenic mouse vector, produced multiple lines of transgenic mice, and bred the *PrP-mAbca1* Tg mice to the PDAPP model of AD. In PDAPP cohorts that overexpressed ABCA1 by 2-fold or more, we observed not only decreased Aβ deposition, but also a dramatic decrease in fibrillar Aβ. Overall, these data demonstrate that selective overexpression of ABCA1 is sufficient to decrease the deposition and fibrillogenesis of Aβ in the brain, likely by increasing the lipidation of apoE-containing lipoproteins in the CNS.

Results

Creation and characterization of PrP-mAbca1 Tg mice. Thirteen founders tested positive for the *PrP-mAbca1* transgene by PCR. One founder died before breeding, 1 founder was sterile, 3 founders failed to exhibit germline transmission of the transgene, and 1 founder did not show overexpression of ABCA1 in the brain. The 7 remaining founders (designated B, D, E, G, I, J, and L) all produced pups that were positive for the *PrP-mAbca1* transgene and demonstrated ABCA1 overexpression in the brain. The progeny of 5 founders bred well and were used for experiments (lines D, E, L, J, and G).

The 5 lines of *PrP-mAbca1* Tg mice that we examined had different levels of ABCA1 overexpression in the cortex, ranging from approximately 2-fold in line D to approximately 14-fold in line G (Figure 1A). Analysis of tissue from the occipital cortex, frontal cortex, hippocampus, cerebellum, striatum, septum, and thalamus showed that *PrP-mAbca1* Tg mice overexpressed ABCA1 throughout the brain (Figure 1B).

Representative tissues from the major organ systems were collected to determine the extent of ABCA1 overexpression throughout the body. Using Western blot analyses, we detected high endogenous mouse ABCA1 expression in lung, liver, spleen, bladder, testis, and brain (Figure 1C, middle panel). In comparison, high expression of the *PrP-mAbca1* transgene was found in the brain, as well as in kidney, testis, and muscle (Figure 1C, upper panel). Since the *PrP-mAbca1* Tg mice used in these experiments express endogenous ABCA1 in addition to the *PrP-mAbca1* transgene, they have normal to increased ABCA1 activity in organs outside the brain.

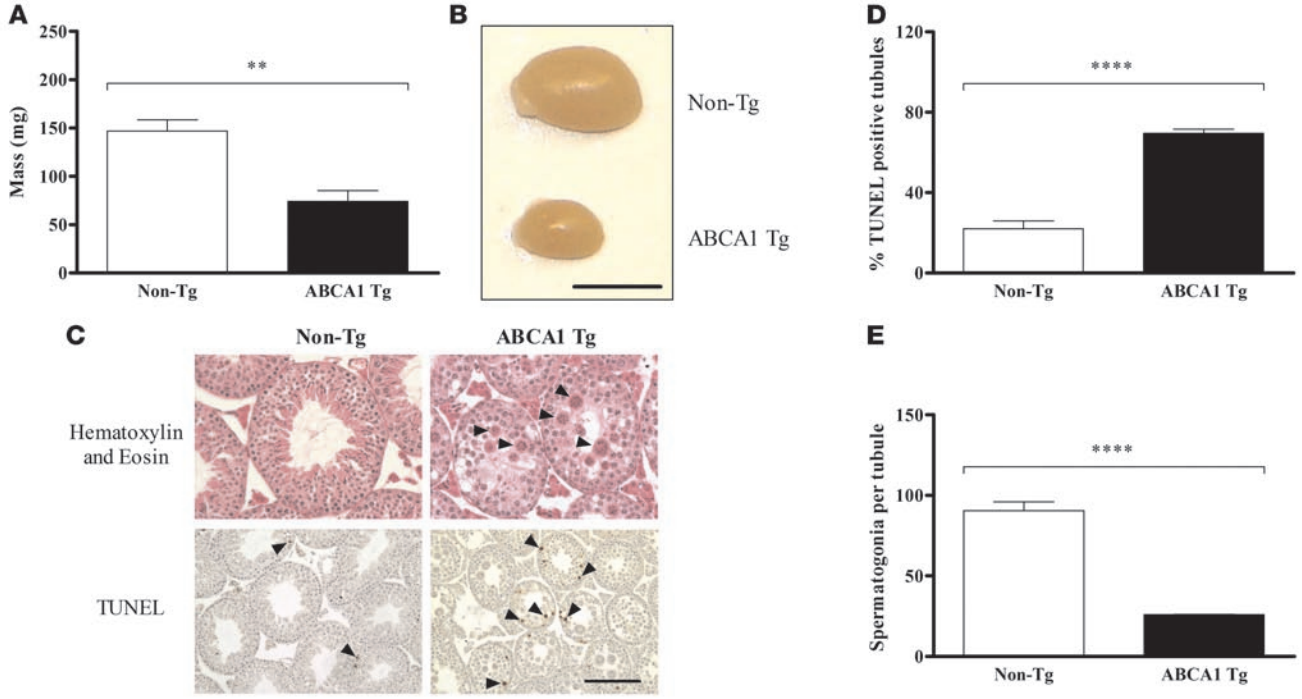

Figure 2

Spermatogenesis defects in 3-month-old *PrP-mAbca1* line E Tg mice. (**A**) Testes from *PrP-mAbca1* line E mice ($n = 5$) and non-Tg mice ($n = 6$) were dissected and weighed. (**B**) A representative testis from a Tg mouse and a non-Tg mouse. Scale bar: 5 mm. (**C**) H&E-stained sections show normal testicular histology in non-Tg mice (top left panel) and marked degeneration of seminiferous tubules of Tg mice (top right panel), with several multinucleated giant cells (arrowheads) present in almost every tubule compared with their rare occurrence in non-Tg mice. No elongated spermatids were present in testes from Tg mice. TUNEL staining shows occasional apoptotic cells in testes from non-Tg mice (bottom left panel) and frequent apoptotic cells in testes from Tg mice (bottom right panel). Scale bar: 50 μm for the top panels and 100 μm for the bottom panels. (**D**) Quantification of TUNEL staining in the testes of Tg ($n = 4$) and non-Tg littermate control mice ($n = 4$). (**E**) Sections of testes from Tg ($n = 3$) and non-Tg littermate control mice ($n = 4$) underwent immunohistochemical staining with an anti-GCNA1 antibody that stains germ cells. The number of GCNA1-positive cells per tubule was tabulated. Statistical analyses of differences between Tg and non-Tg mice were performed using 2-tailed Student's *t* test. $^{**}P < 0.01$; $^{****}P < 0.0001$.

The 5 *PrP-mAbca1* Tg lines we studied produced equal numbers of male and female pups with no overt differences in growth or health. However, male mice from all but the lowest overexpressing line (line D) were sterile. Gross examination of the testes from *PrP-mAbca1* line E mice revealed severe atrophy in Tg mice, with an approximately 50% reduction in testes mass compared with non-Tg mice (Figure 2, A and B). To further characterize this phenotype, we performed histological examination of the testes of Tg and non-Tg mice. Compared with non-Tg mice (Figure 2C, top left panel), the seminiferous tubules of the testes from the Tg mice showed atrophy with marked degenerative changes highlighted by a large increase in multinucleated giant cells and cells with condensed nuclei (Figure 2C, top right panel). These degenerative changes were present in almost every section of the seminiferous tubules in the Tg testes compared with their rare presence in the non-Tg testes. TUNEL staining showed approximately 3-fold more apoptotic cells in testes from Tg mice (Figure 2C, bottom right panel), as compared with non-Tg mice (Figure 2C, bottom left panel, and Figure 2D). Further, testes from Tg mice exhibited maturation arrest due to absence of mature products of spermatogenesis such as elongated spermatids and spermatozoa (Figure 2C, top right panel). These findings are consistent with the marked reduction in germ cells detected by immunohistochemistry with an anti-GCNA1 antibody (Figure 2E). The numbers of Sertoli cells, detected by GATA4 immunohistochemistry, were similar in Tg and wild-type testes (data not shown). A previous study has shown that *Abca1*$^{-/-}$ mice have abnormalities in sperm production (28), and our data suggest that an excess of ABCA1 is also detrimental to male fertility. However, previous reports on other ABCA1 Tg mice have not reported any abnormalities in testicle size or male fertility (25, 27, 29). It is interesting that the spermatogenesis defects reported here are highly similar to those observed in mice with aberrant glial cell line–derived neurotrophic factor–Ret receptor tyrosine kinase (GDNF/Ret) signaling (30, 31). Thus, it is possible that ABCA1 activity directly or indirectly influences the GDNF/Ret signaling system in the testes.

Amyloid deposition in the brains of PDAPP/Abca1 Tg mice. Mice from *PrP-mAbca1* lines D, E, and J, which overexpressed mABCA1 by approximately 2-, 6-, and 12-fold, respectively, were bred to the PDAPP mouse model of AD. The resulting PDAPP/*Abca1* Tg mice and their PDAPP/*Abca1* non-Tg littermates were sacrificed at either 3 or 12 months. Brain sections from 12-month-old PDAPP/*Abca1* line E mice were stained for Aβ. The PDAPP mice with wild-type ABCA1 levels (PDAPP/*Abca1* non-Tg mice) had frequent punctate Aβ deposits in the cortex and hippocampus (Figure 3A, top left panel), including the molecular layer of the hippocampus, but almost no Aβ deposits in the hilus of the dentate gyrus of the hippocampus (Figure 3A, middle left panel). In contrast, the PDAPP

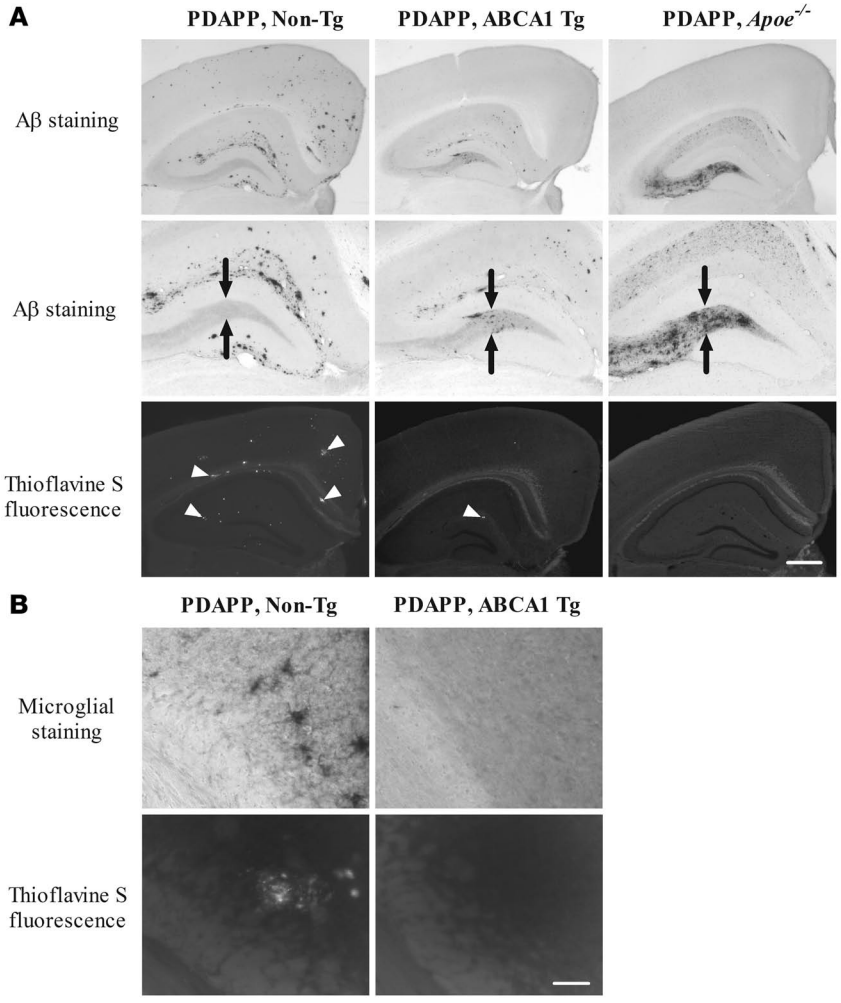

Figure 3
Aβ staining and thioflavine S fluorescence in the brains of 12-month-old PDAPP/*Abca1* line E mice. (**A**) Sections of brain from PDAPP/*Abca1* non-TG mice, PDAPP/*Abca1* line E mice, and PDAPP/*Apoe*$^{-/-}$ mice were stained for Aβ using the 3D6 antibody. True amyloid was visualized by thioflavine S fluorescence. The arrows shown in the middle panels indicate the upper and lower limits of the hilus of the dentate gyrus. Scale bar: 125 μm for the top and bottom panels and 250 μm for the middle panels. (**B**) Brain sections from PDAPP/*Abca1* line E mice were immunostained with an antibody against the microglial marker CD45. Scale bar: 625 μm for all panels.

mice with ABCA1 overexpression (PDAPP/*Abca1* Tg mice) had rare Aβ deposition in the cortex (Figure 3A, top middle panel), occasional Aβ deposition in the molecular layer, and frequent Aβ deposition in the hilus of the dentate gyrus (Figure 3A, middle panel). This is interesting because PDAPP mice rarely deposit Aβ in the hilus of the dentate gyrus unless they also lack *Apoe* (Figure 3A, top right and middle right panels) (32–34).

Brain sections from the 12-month-old mice were also stained with thioflavine S to detect fibrillar Aβ. As detected via fluorescence microscopy, frequent amyloid plaques were seen in the cortex and hippocampus of the PDAPP/*Abca1* non-Tg mice (Figure 3A, bottom left panel). However, almost no thioflavine S–positive amyloid plaques were seen in the PDAPP/*Abca1* Tg mice (Figure 3A, bottom middle panel) or in PDAPP/*Apoe*$^{-/-}$ mice (Figure 3A, bottom right panel), even in sections with extensive Aβ deposits. This demonstrates that Aβ deposits in the PDAPP/*Abca1* Tg mice are almost all diffuse, with very little true amyloid. In the PDAPP/*Abca1* Tg mice, the preferential deposition of Aβ in the hilus of the dentate gyrus of the hippocampus, along with the lack of thioflavine S–positive Aβ deposits, is virtually identical to the pattern of Aβ deposition in PDAPP/*Apoe*$^{-/-}$ mice. This suggests that increasing ABCA1-mediated lipidation of apoE has an effect on Aβ deposition very similar to that seen in APP Tg mice lacking apoE.

Consistent with previous work (35), the thioflavine S–positive plaques in the brains of PDAPP/*Abca1* non-Tg mice were associated with clusters of reactive microglia (Figure 3B, upper left and lower left panels). The PDAPP/*Abca1* Tg mice, which had very few thioflavine S–positive deposits, had few to no observable clusters of reactive microglia in their brains (Figure 3B, upper right and lower right panels). These findings demonstrate that the paucity of fibrillar Aβ in the brains of PDAPP/*Abca1* Tg mice is associated with decreased microglial activation.

Quantitative stereological analyses of Aβ deposition demonstrated markedly and significantly lower Aβ load in the cortex of 12-month-old PDAPP/*Abca1* Tg mice as compared with PDAPP/*Abca1* non-Tg littermate control mice (Figure 4A). The Aβ load in the entire hippocampus did not vary significantly according to the presence of the mABCA1 transgene, but the distribution of Aβ within the hippocampus was altered by the transgene. PDAPP/*Abca1* Tg mice had more Aβ deposition in the hilus of the dentate gyrus and less in the molecular layer (Figure 4A). Quantification of thioflavine S–positive amyloid plaques confirmed the near absence of true amyloid plaques in PDAPP/*Abca1* Tg mice, in contrast to the robust presence of amyloid plaques in PDAPP/non-Tg mice (Figure 4B). Furthermore, thioflavine S–positive amyloid plaques were quantified in PDAPP/*Abca1* lines D, E, and J, which overexpress ABCA1 by 2-, 6-, and 12-fold in the brain, respectively. Two-fold overexpression of ABCA1 in the brain decreased deposition of thioflavine S–positive amyloid by approximately 50%. Overexpression of ABCA1 by 6-fold or more decreased deposition of thioflavine S–positive amyloid to almost 0. These data demonstrate that overexpression of ABCA1 protects PDAPP mice from developing thioflavine S–positive amyloid plaques.

The amount of Aβ in the brains of the PDAPP/*Abca1* mice was quantified by ELISA at 3 months of age, when Aβ had not yet deposited, and after 12 months, when extensive Aβ deposition had occurred. At 3 months of age, both the PDAPP/*Abca1* line D and line E Tg mice, which overexpress ABCA1 by 2- and 6-fold, respectively, had significantly (15%–50%) higher Aβ levels than non-Tg littermate control mice (Figure 5, A and B, and Table 1). These higher levels do not represent deposited Aβ, as the mice did not have histological evidence of Aβ deposition at this age. To determine whether the Aβ levels in the young PDAPP/*Abca1* Tg mice

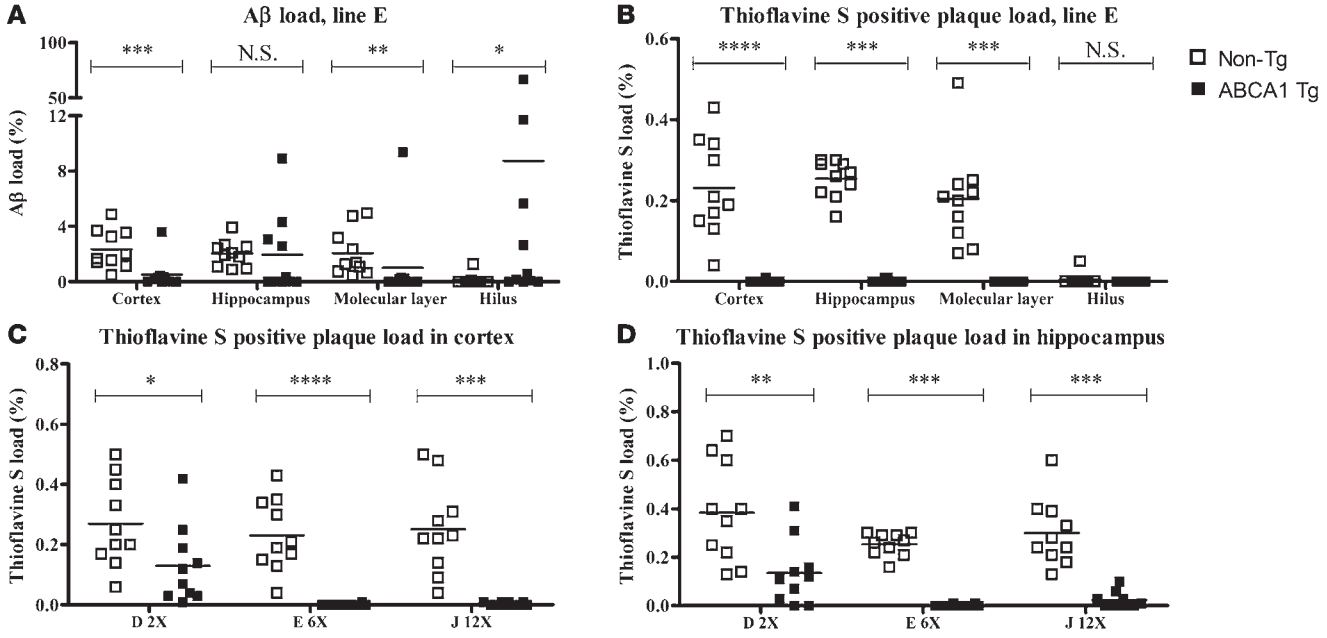

Figure 4

Aβ load and thioflavine S–positive plaque load in 12-month-old PDAPP/*Abca1* mice. (**A** and **B**) Using stereological methods, Aβ staining and thioflavine S fluorescence were quantified in the cortex, hippocampus, and 2 subregions of the hippocampus (molecular layer and hilus of the dentate gyrus) of PDAPP/*Abca1* line E mice. (**C** and **D**) Thioflavine S fluorescence was quantified in the cortex and hippocampus of PDAPP/*Abca1* line D, line E, and line J mice. $n = 10$ for all groups. Statistical analyses of differences between Tg and non-Tg mice were performed using the Mann-Whitney *U* test. $^*P < 0.05$; $^{**}P < 0.01$; $^{***}P < 0.001$; $^{****}P < 0.0001$.

were higher due to increased Aβ generation from APP, levels of APP and the C-terminal fragments (CTFs) created by enzymatic cleavage of APP were assessed by Western blotting. There were no differences between PDAPP/*Abca1* line E Tg and PDAPP/non-Tg mice (Figure 5E), suggesting that Aβ production was not likely to account for the differences in Aβ levels at 3 months. Previously, our group found that PDAPP/*Apoe*$^{-/-}$ mice also have higher brain Aβ levels at 3 months of age, probably because apoE is required for normal transport and clearance of soluble Aβ (36).

By 12 months of age, large amounts of Aβ had accumulated in the brains of all mice with the PDAPP transgene (more than 100-fold compared with 3 months of age). However, mice that also overexpressed ABCA1 developed significantly less Aβ deposition than non-Tg littermates. Aβ levels in PDAPP/*Abca1* line D Tg mice were approximately 2.5-fold lower compared with those in PDAPP/non-Tg littermate control mice (Figure 5C and Table 1), and the PDAPP/*Abca1* line E Tg mice had approximately 3-fold less Aβ in the brain compared with PDAPP/non-Tg littermate control mice (Figure 5D and Table 1). PDAPP/*Abca1* line J Tg mice had a decrease in Aβ levels at 12 months of age similar to that seen in PDAPP/*Abca1* line E Tg mice (data not shown). As shown in previous studies, PDAPP/*Apoe*$^{-/-}$ mice also develop approximately 2- to 3-fold less Aβ deposition than PDAPP/*Apoe*$^{+/+}$ mice (32–34). Thus, the PDAPP/*Abca1* Tg mice have a phenotype similar to that seen in PDAPP/*Apoe*$^{-/-}$ mice.

ApoE levels and solubility in PrP-mAbca1 Tg mice. Previously, we and others found that *Abca1*$^{-/-}$ mice have reduced levels of apoE in the CNS (18–20). This may reflect increased brain catabolism of poorly lipidated apoE produced in the absence of ABCA1, similar to the rapid turnover of poorly lipidated peripheral apoA-I in ABCA1-deficient states. We hypothesized that excess ABCA1 function in the *PrP-mAbca1* Tg mice would result in increased apoE lipidation, which would decrease apoE catabolism. Theoretical support for this hypothesis was given by the elevated levels of HDL-associated apolipoproteins in the plasma of previously generated ABCA1 Tg models (25, 27). Although we expected that the *PrP-mAbca1* Tg mice would have increased levels of apoE in the CNS compared with non-Tg littermate controls, this was not the case. While 2-fold overexpression of ABCA1 in *PrP-mAbca1* line D Tg mice did not result in altered apoE levels (Figure 6A), overexpression of ABCA1 by 6-fold or greater resulted in reductions in hippocampal apoE of approximately 40% compared with non-Tg littermate control mice (Figure 6A). The size of the decrease did not vary between lines that overexpressed ABCA1 6-fold to 14-fold, indicating that the effect is saturable. Also, the extent that ABCA1 overexpression results in lower levels of apoE varies according to brain region. In the cortex, apoE was decreased by only approximately 20% in Tg mice from *PrP-mAbca1* lines L, J, and G and was not decreased significantly in lines D or E (Figure 6B). In the CSF, apoE levels were decreased by approximately 40%–70% in all lines overexpressing ABCA1 (Figure 6C). PDAPP/*Abca1* Tg mice with 6-fold or greater levels of overexpression also had lower levels of apoE in the brain at 3 months of age, and the amount of this change was not different from that in non-PDAPP mice (data not shown). To determine whether the decreased apoE levels in the *PrP-mAbca1* Tg mice were due to decreased transcription of apoE, we performed real-time quantitative RT-PCR to determine the relative levels of apoE mRNA in *PrP-mAbca1* line E and line J mice. We found no difference between Tg and non-Tg apoE mRNA levels in either the hippocampus or cortex of either line (Figure 6D and data not shown). In addition to decreasing apoE levels, overexpression of ABCA1

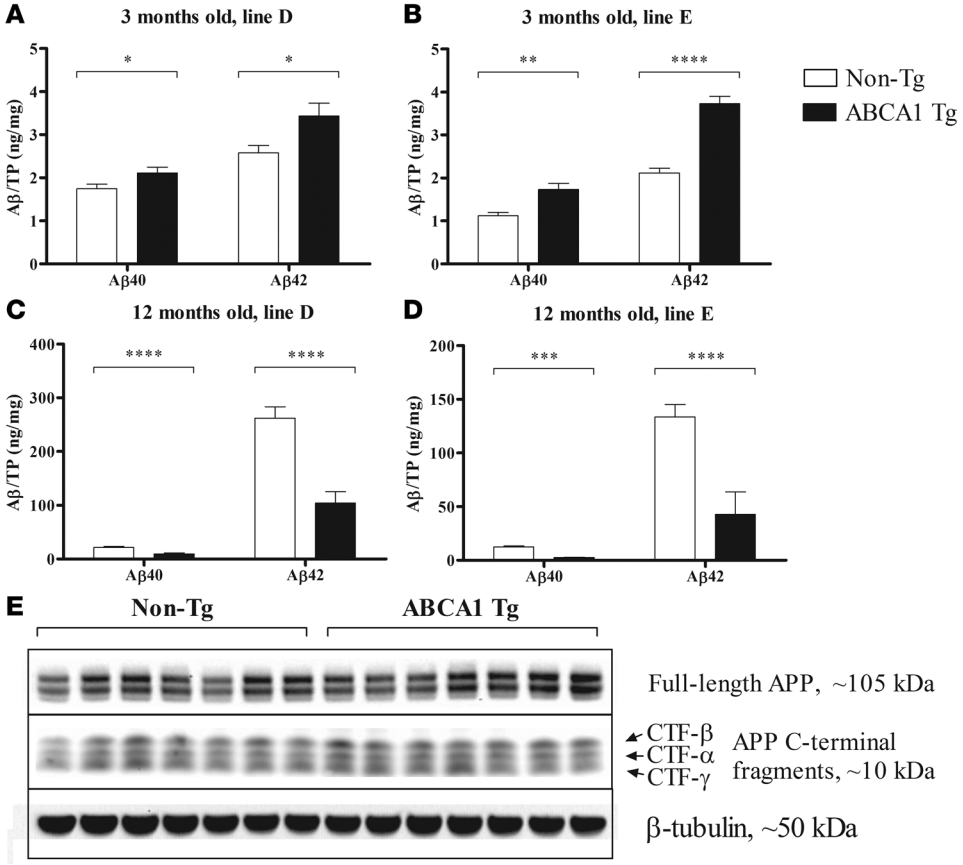

Figure 5
Aβ as detected by ELISA in the hippocampus of PDAPP/*Abca1* mice. (**A**–**D**) Aβ was serially extracted from the hippocampus using carbonate and guanidine buffers and measured by ELISA. The Aβ in the carbonate and guanidine extracts was summed, and total Aβ40 and Aβ42 ares represented. TP, total protein in the tissue lysate. (**A** and **B**) Aβ in the hippocampus of 3-month-old mice from PDAPP/*Abca1* lines D and E, respectively. $n = 11$ in all groups. (**C** and **D**) Aβ in the hippocampus of 12-month-old mice from PDAPP/*Abca1* lines D and E, respectively. $n = 10$–14 in all groups. Statistical analyses of differences between Tg and non-Tg mice were performed using 2-tailed Student's *t* test. $^{*}P < 0.05$; $^{**}P < 0.01$; $^{***}P < 0.001$; $^{****}P < 0.0001$. (**E**) Levels of APP and APP C-terminal fragments in hippocampus from PDAPP/*Abca1* line E mice were visualized by Western blotting. $n = 7$ for both groups. β-Tubulin was used as a loading control. Quantification of the APP and CTF bands using image analysis software revealed no significant differences between PDAPP/*Abca1* Tg and PDAPP/*Abca1* non-Tg mice.

affected the biochemical properties of apoE. In all groups of *PrP-mAbca1* Tg mice that overexpressed ABCA1 by 6-fold or greater, approximately twice as much apoE in the hippocampus and cortex was insoluble in carbonate buffer and required 5 M guanidine for extraction compared with non-Tg littermate control groups (data not shown). The relative insolubility of brain-associated apoE from *PrP-mAbca1* mice in carbonate buffer suggests a difference in apoE metabolism induced by ABCA1 overexpression.

Plasma levels of cholesterol and apoE were measured in 3-month-old mice of *PrP-Abca1* lines D, E, L, J, and G. No differences in plasma apoE levels between Tg and non-Tg mice were observed except in line J, the second-highest-expressing line, which exhibited elevated plasma apoE levels of 97 ± 6 μg/ml in Tg mice compared with 78 ± 6 μg/ml in non-Tg mice (mean ± SEM; $P = 0.04$). Plasma cholesterol levels were also not different between Tg and non-Tg mice except for the 2 highest-expressing lines (J and G), which had higher plasma cholesterol than non-Tg mice. In *PrP-Abca1* line J mice, levels of plasma cholesterol were 647 ± 47 μg/ml in Tg mice and 348 ± 50 μg/ml in non-Tg mice ($P = 0.0007$). In *PrP-Abca1* line G mice, levels of plasma cholesterol were 586 ± 42 μg/ml in Tg mice and 418 ± 48 μg/ml in non-Tg mice ($P = 0.02$). These findings suggest that integration of multiple copies of the *PrP-mAbca1* transgene can affect peripheral cholesterol metabolism through mechanisms that remain to be identified. In addition to plasma cholesterol, plasma HDL was assessed in Tg and non-Tg mice by fractionating plasma from 3-month-old *PrP-mAbca1* line E mice using size-exclusion gel chromatography. HDL-associated cholesterol and phospholipids were not significantly different in Tg and non-Tg mice. Finally, plasma apoA-I levels were assessed by Western blotting in mAbca1 line E Tg mice versus non-Tg littermates. There was no significant difference between the groups (data not shown).

apoE-containing lipoprotein particles from PrP-mAbca1 Tg mice. We previously found that mice lacking ABCA1 had abnormally small apoE-containing lipoprotein particles in their CSF and that primary astrocyte cultures derived from *Abca1*$^{-/-}$ mice contained small, lipid-poor apoE-containing lipoprotein particles (18). We hypothesized that overexpression of ABCA1 in the brain would result in greater lipidation of apoE-containing lipoprotein particles in the CSF and that primary astrocytes derived from *PrP-mAbca1* Tg mice would secrete larger, more lipid-rich apoE-containing lipoprotein particles. Nondenaturing gradient gel electrophoresis of CSF from *PrP-mAbca1* mice, followed by Western blotting for apoE, was performed. apoE-containing lipoprotein particles from the Tg mice tended to be larger in size than particles from non-Tg mice (Figure 7A). This suggests that apoE particles in the CNS are more lipidated in Tg mice. To further characterize the effects of ABCA1 overexpression on nascent apoE particles, primary cultures of astrocytes were prepared from *PrP-mAbca1* Tg mice and non-Tg littermate control mice and allowed to secrete apoE-containing lipoprotein particles into serum-free media over 72 hours. Astrocyte-conditioned media (ACM) from *PrP-mAbca1* Tg mice and non-Tg littermate controls was then subjected to nondenaturing gradient gel electrophoresis followed by Western blotting for apoE. The apoE-containing lipoprotein particles from the Tg mice had a greater proportion of lipoprotein particles larger than 11 nm than that seen in media derived from non-Tg mice (Figure 7B).

Table 1
Aβ levels in brain extracts as measured by ELISA

	Carbonate		Guanidine		Total	
	Aβ40	Aβ42	Aβ40	Aβ42	Aβ40	Aβ42
3 mo old						
Hippocampus						
Line D						
–, *n* = 11	0.36 ± 0.09[A]	0.34 ± 0.04[B]	1.39 ± 0.30	2.25 ± 0.54[A]	1.75 ± 0.35[A]	2.59 ± 0.55[A]
+, *n* = 11	0.49 ± 0.13	0.47 ± 0.15	1.62 ± 0.35	2.97 ± 0.91	2.12 ± 0.44	3.44 ± 0.98
Line E						
–, *n* = 11	0.32 ± 0.07[B]	0.44 ± 0.10[A]	0.80 ± 0.23[B]	1.68 ± 0.36[C]	1.12 ± 0.26[B]	2.11 ± 0.37[D]
+, *n* = 11	0.41 ± 0.05	0.57 ± 0.12	1.32 ± 0.46	3.17 ± 0.52	1.73 ± 0.48	3.73 ± 0.56
Cortex						
Line D						
–, *n* = 11	0.19 ± 0.05	0.34 ± 0.07	0.45 ± 0.07	0.89 ± 0.12	0.64 ± 0.11	1.23 ± 0.13
+, *n* = 11	0.23 ± 0.09	0.35 ± 0.08	0.05 ± 0.07	0.86 ± 0.13	0.73 ± 0.12	1.21 ± 0.11
Line E						
–, *n* = 11	0.35 ± 0.05	0.34 ± 0.04	0.26 ± 0.04[C]	0.97 ± 0.16[D]	0.60 ± 0.07[C]	1.31 ± 0.15[D]
+, *n* = 11	0.40 ± 0.08	0.38 ± 0.05	0.45 ± 0.13	1.66 ± 0.32	0.85 ± 0.19	2.04 ± 0.32
12 mo old						
Hippocampus						
Line D						
–, *n* = 12	0.86 ± 0.25[C]	2.03 ± 0.47[D]	21.1 ± 5.2[D]	260 ± 73[D]	22.0 ± 5.4[D]	262 ± 73[D]
+, *n* = 12	0.49 ± 0.13	0.93 ± 0.36	9.14 ± 4.72	103 ± 73	9.63 ± 4.81	104 ± 73
Line E						
–, *n* = 14	0.59 ± 0.12[B]	1.52 ± 0.44[D]	12.0 ± 2.6[D]	132 ± 43	12.6 ± 2.7[D]	134 ± 44[C]
+, *n* = 10	0.46 ± 0.08	0.55 ± 0.41	2.34 ± 0.31	42.3 ± 65.8	2.80 ± 0.33	42.8 ± 66.2
Cortex						
Line D						
–, *n* = 12	0.47 ± 0.15[B]	1.42 ± 0.49[C]	5.95 ± 2.16[C]	81.0 ± 34.3[C]	6.42 ± 2.27[C]	81.0 ± 34.3[C]
+, n = 12	0.31 ± 0.10	0.70 ± 0.26	3.29 ± 0.84	33.8 ± 11.1	3.60 ± 0.86	33.8 ± 11.1
Line E						
–, *n* = 14	0.34 ± 0.07	0.83 ± 0.24[D]	3.51 ± 1.15[D]	46.0 ± 22.4[B]	3.84 ± 1.18[D]	46.9 ± 22.5[B]
+, *n* = 10	0.29 ± 0.05	0.40 ± 0.15	1.38 ± 0.18	15.6 ± 21.9	1.66 ± 0.19	16.0 ± 22.0

Units are ng of Aβ per mg of total protein. Statistical analyses of differences between Tg and non-Tg mice were performed using 2-tailed Student's *t* test. No footnote, not significant; [A]$P < 0.05$; [B]$P < 0.01$; [C]$P < 0.001$; [D]$P < 0.0001$.

To determine whether the astrocyte-derived apoE-containing lipoprotein particles from *PrP-mAbca1* mice contained more lipid, ACM was subjected to size-exclusion gel chromatography to separate the different classes of lipoproteins. Compared with astrocytes derived from non-Tg mice, astrocytes derived from Tg mice secreted less apoE and associated cholesterol in HDL-like lipoproteins (Figure 7, C and D). However, within the lipoprotein fractions, there was a significantly greater ratio of cholesterol to apoE (Figure 7E). This demonstrates that ABCA1 overexpression resulted in increased lipidation of nascent apoE particles.

Effects of brain overexpression of ABCA1 on other proteins. We used Western blotting of ABCA1 Tg line E brain lysates to assess whether overexpression of mAbca1 influenced the levels of other proteins that are potentially involved in apoE and Aβ metabolism. No differences were found in the levels of low-density lipoprotein receptor (LDLR), LDLR-related protein 1 (LRP1), and apoA-I when comparing ABCA1 line E Tg mice to non-Tg littermates (Figure 8, A and B). The level of ABCG1 in brain lysates was also compared by Western blot in samples from multiple *mAbca1* transgenic lines, and there was no consistent difference found between *mAbca1* Tg and non-Tg mice (data not shown). However, levels of apoJ (also called clusterin) were significantly lower in *PrP-mAbca1* line E Tg brain lysates versus non-Tg control brain lysates (Figure 8, A and B). Because this difference in apoJ levels was not observed in ABCA1 line D mice (data not shown), a 2-fold overexpression of ABCA1 in the brain is insufficient to significantly alter either apoJ or apoE levels (Figure 6A). However, lines with greater than 2-fold ABCA1 overexpression exhibited changes in both apoE and apoJ levels. Notably, because 2-fold overexpression of ABCA1 was sufficient to reduce Aβ levels in PDAPP/*Abca1* line D mice (Figure 5, A and C) without significant alterations in either apoE or apoJ levels, the beneficial effects of excess ABCA1 function in Aβ reduction appear to be largely independent of the absolute levels of apoE and apoJ.

Discussion

Our laboratory and others previously showed that ABCA1-deficient mice have decreased levels and poor lipidation of apoE in the CNS (18–20). Further, when APP Tg mice were bred with *Abca1*$^{-/-}$ mice, the APP Tg, *Abca1*$^{-/-}$ mice developed increased Aβ accumulation and amyloid deposition (20, 23). This result is consistent with the hypothesis that poorly lipidated apoE is highly amyloidogenic. In the current study, we hypothesized that overexpression of

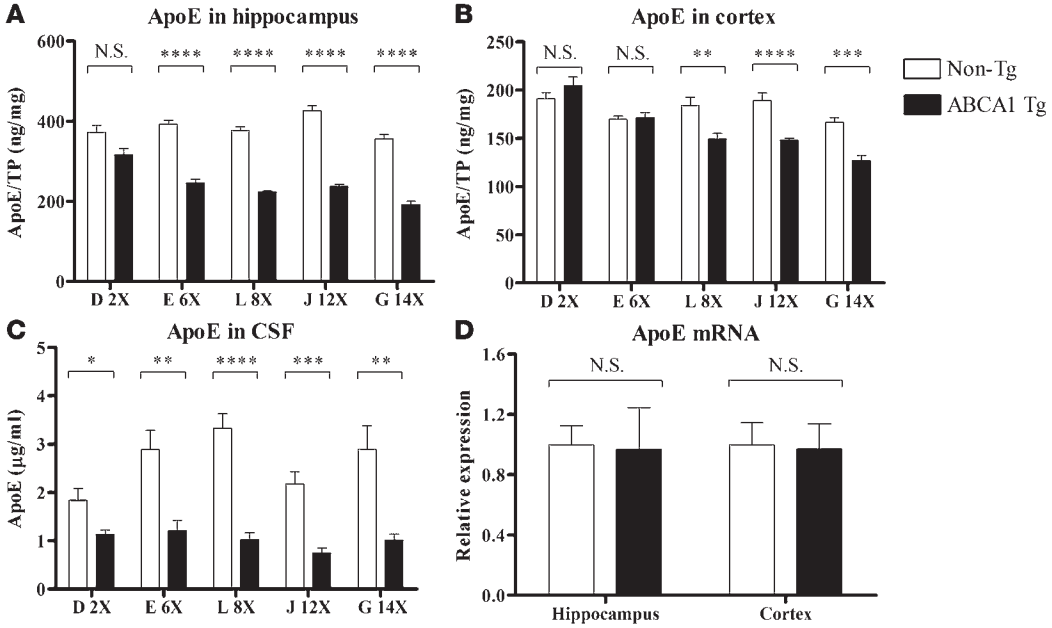

Figure 6

Levels of apoE in the hippocampus, cortex, and CSF of 3-month-old *PrP-mAbca1* Tg mice. (**A** and **B**) apoE was serially extracted from brain tissue using carbonate and guanidine buffers and measured by ELISA. The apoE in the carbonate and guanidine extracts was summed, and total apoE is represented in **A** and **B**. (**C**) CSF was diluted, and apoE levels were measured by ELISA. (**D**) RNA was extracted from the hippocampus and cortex of *PrP-mAbca1* line E mice. Real-time quantitative RT-PCR was performed for mouse apoE mRNA and total rRNA. Mouse apoE mRNA was normalized to total rRNA. (**A**–**D**) For all groups, the n = 7–9. Tg and non-Tg samples from the same line were processed at the same time. Statistical analyses of differences between Tg and non-Tg mice were performed using 2-tailed Student's t test. *$P < 0.05$; **$P < 0.01$; ***$P < 0.001$; ****$P < 0.0001$.

ABCA1 in the brain would increase apoE lipidation, thereby leading to decreased amyloid deposition. To address this hypothesis, we created several lines of *PrP-mAbca1* Tg mice that overexpress ABCA1 2- to 14-fold in the brain and bred them to the PDAPP mouse model of AD. We found that PDAPP/*Abca1* Tg mice had (a) decreased deposition of Aβ; (b) a near absence of thioflavine S–positive amyloid plaques; and (c) a redistribution of Aβ deposits in the hippocampus from the molecular layer to the hilus of the dentate gyrus. While alterations of genes and proteins such as secretases, Aβ-degrading enzymes, and chaperones have been shown to modify Aβ deposition, this triad of findings described above has only been described in APP Tg mice that lack apoE (32–34, 37). This phenotype strongly argues that overexpression of ABCA1 in the brain decreases the amyloidogenic properties of apoE and, further, that increased apoE lipidation results in a phenotype very similar to apoE deficiency with respect to Aβ metabolism. These findings suggest that specifically increasing ABCA1 function or expression should be explored as a target for AD therapeutics.

The apoE isoform is a major genetic risk factor for AD and cerebral amyloid angiopathy (CAA) (38–40). The apoE4 isoform increases risk and apoE2 decreases risk for AD (41). *APOE* was discovered to be a genetic risk factor for AD after apoE was found to be a major binding protein for Aβ in human CSF (38, 42). The role of apoE in the aggregation, deposition, and conformation of Aβ in the brain in vivo was first shown when APP Tg mice were crossed to *Apoe*$^{-/-}$ mice. The phenotype in these mice was striking and similar to the phenotype observed in the Abca1 Tg mice described here. In APP Tg mice, the onset of Aβ deposition was unaffected by the presence or absence of apoE; however, in the absence of apoE, there was less Aβ accumulation both histologically and biochemically. Further, throughout the lifespan of APP Tg, *Apoe*$^{-/-}$ mice, very few to no fibrillar Aβ deposits including neuritic plaques, CAA, or CAA-associated hemorrhage ever developed (32, 33, 43, 44). Also, in PDAPP/*Apoe*$^{-/-}$ mice, there was a redistribution of Aβ deposits in the hippocampus to the hilus of the dentate gyrus, where these deposits are not normally found (34, 37, 45). This cluster of phenotypes has not been seen in mice with other modifications to APP/Aβ, including elimination of β-secretase or increasing an Aβ protease such as neprilysin (46, 47). The closest phenotype to that of APP/*Apoe*$^{-/-}$ mice is seen in APP Tg mice that lack apoJ, also called clusterin. However, PDAPP/*clusterin*$^{-/-}$ mice do not redistribute Aβ to the hilus or exhibit nearly as dramatic a decrease in fibrillar Aβ plaques (48) as either *Apoe*$^{-/-}$ or *Abca1* Tg mice. The fact that PDAPP Tg mice crossed with *PrP-mAbca1* Tg mice have a phenotype virtually identical to that seen in PDAPP/*Apoe*$^{-/-}$ mice strongly argues that the effect of ABCA1 on Aβ related pathology is via altering the properties of apoE. Intriguingly, the functional effect of increasing apoE lipidation is strikingly similar to that of deleting apoE, with respect to Aβ fibrillization, deposition, or clearance.

There are several additional findings that support the idea that overexpression of ABCA1 influences Aβ metabolism via apoE. We previously found that when PDAPP/*Apoe*$^{-/-}$ mice are 3 months of age, prior to Aβ deposition, they have an approximately 2-fold increase in the level of Aβ in soluble brain homogenates and brain interstitial fluid (36). This is similar to what we observed in 3-month-old PDAPP/*Abca1* Tg mice. Our previous studies in PDAPP/*Apoe*$^{-/-}$ mice showed that the increase in interstitial fluid Aβ observed early in life was due to apoE's ability to influence Aβ

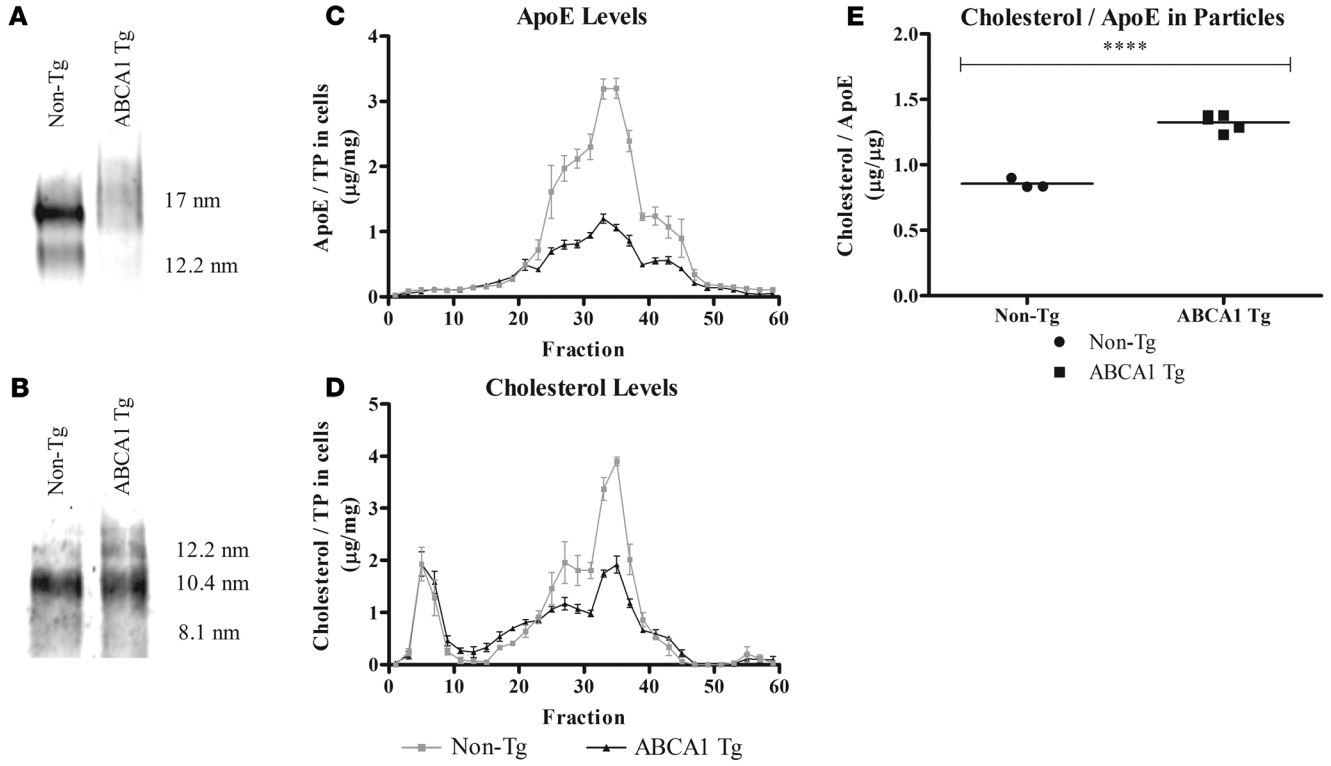

Figure 7

Analysis of apoE-containing lipoprotein particles derived from *PrP-mAbca1* line E mice. (**A**) CSF (2 μl) from 3-month-old *PrP-mAbca1* line E mice was run on a nondenaturing gradient gel, and Western blot analysis for mouse apoE was performed. (**B**) Media conditioned by primary astrocytes derived from *PrP-mAbca1* line E mice was run on a nondenaturing gradient gel, and Western blot analysis for mouse apoE was performed. Samples containing equal amounts of apoE were loaded. (**C** and **D**) Primary astrocytes derived from *PrP-mAbca1* line E mice secreted apoE-containing lipoprotein particles into the media over 72 hours. Lipoprotein particles in the ACM were separated by size using gel filtration chromatography. The levels of apoE and cholesterol were then measured in the fractions and normalized to total protein in the cell pellet. $n = 3$ for non-Tg and $n = 5$ for Tg. (**E**) The amount of cholesterol and apoE in lipoprotein fractions 20–50 was totaled, and lipoprotein cholesterol was divided by lipoprotein apoE. Two-tailed Student's *t* test was performed to evaluate the statistical significance of differences between particles from Tg and non-Tg mice. ****$P < 0.0001$.

transport or clearance (36). Thus, the fact that *Apoe*$^{-/-}$ mice did not have accelerated Aβ deposition, in spite of higher soluble Aβ early in life, is likely due to the removal of apoE and its function as an Aβ binding molecule or pathological chaperone. The overexpression of ABCA1 that resulted in apoE-containing particles with a larger size than normal may have resulted in an alteration in the ability of apoE to influence the time of onset of Aβ aggregation via an effect on Aβ binding that subsequently influenced Aβ clearance or fibrillogenesis. For example, recent experiments suggest that when Aβ is injected in the brain alone, it is rapidly cleared from the brain, but injection of Aβ together with astrocyte-derived apoE results in greater Aβ retention in the brain (49). It is possible that highly lipidated apoE may increase Aβ transport from brain to blood or alter local Aβ clearance in such a way as to decrease the probability of Aβ aggregation. These ideas can be directly tested in future experiments.

While we did observe lower levels of apoE in some Abca1 Tg lines, this was not seen in the *PrP-mAbca1* line D or in the cortex of the *PrP-mAbca1* line E mice. The observation that there were lower levels of apoE in the Abca1 Tg lines with high expression suggests that increased lipidation of apoE may promote its uptake by members of the LDLR family. However, since the effect of ABCA1 overexpression on Aβ accumulation and deposition was still marked even in *PrP-mAbca1* line D, which did not have lower apoE levels in the brain, it does not appear that lowered apoE levels are responsible for the effects on Aβ that we observed. It is also unlikely that the effects of ABCA1 overexpression or *Apoe* in APP Tg mice are due to altered Aβ synthesis, as we found no change in total APP or APP C-terminal fragments in PDAPP/*Abca1* Tg mice. There are also no changes in APP levels or APP C-terminal fragments observed in *Apoe*$^{-/-}$ mice (36). Thus, changes in Aβ production are not likely to account for the changes we observed in Aβ levels in PDAPP/*Abca1* Tg mice.

Our data suggest that treatments that increase the expression of ABCA1 would likely decrease Aβ deposition, especially fibrillar Aβ. Activation of the transcription factor LXR has been shown to increase transcription of ABCA1 and many other genes involved in lipid metabolism and other pathways (50–52). LXR agonists have been shown in both in vitro and in vivo experiments to affect Aβ levels (20, 53–57). Whether the effects of LXR agonists on human Aβ levels and ultimately deposition in vivo require ABCA1 remains to be determined.

In addition to the positive effects of overexpression of ABCA1 on Aβ, we did observe that male mice overexpressing ABCA1 at levels 6-fold or greater than those in normal brain were infertile. This is probably due to overexpression of ABCA1 in the testes, which

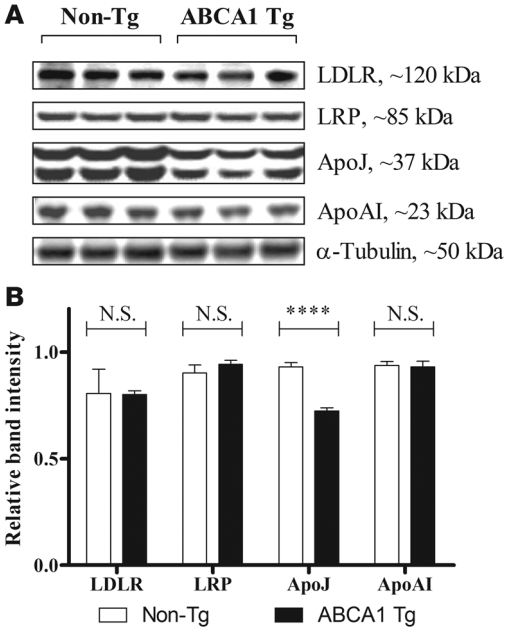

Figure 8

Comparison of lipoprotein receptors and lipoproteins in *PrP-mAbca1* line E Tg versus non-Tg mice. (**A**) Samples of cortex from 3-month-old mice were lysed in RIPA buffer. Equal amounts of total protein from each mouse were loaded into each well of the gel and then assessed by Western blotting for LDLR, LRP, apoJ, apoA-I, and tubulin. Three representative lanes are shown for Tg and non-Tg mice. (**B**) Quantitative analysis of Western blots was performed using Kodak Image Station software, with $n = 3–6$ per group. ****$P < 0.0001$.

occurs throughout the entire lifetime of the *PrP-mAbca1* Tg mice. It is not clear whether an increase in ABCA1 in adulthood may compromise male fertility or whether it may be possible to selectively target expression of ABCA1 in the brain versus testes versus other organs using small molecules. These issues remain to be considered as ABCA1-directed therapies are developed.

The findings that selective ABCA1 deficiency promotes amyloidogenesis whereas selective ABCA1 overexpression lowers amyloid load demonstrates that ABCA1 is a key regulator of Aβ aggregation and deposition. The ABCA1/apoE/Aβ axis is therefore an important area for further investigation. It would be helpful to understand whether overexpression of ABCA1 directly results in altered Aβ transport or clearance in vivo as has been shown in *Apoe*$^{-/-}$ mice. It would also be important to know how increased lipidation of brain-derived apoE influences the ability of apoE-containing lipoproteins to interact with Aβ. Previous in vitro work has shown that lipidated apoE forms an SDS-stable complex with Aβ to a greater extent than nonlipidated apoE (58, 59). In addition, lipidated apoE binds with a much higher affinity than poorly lipidated apoE to soluble Aβ (60). In future experiments, it may be important to utilize apoE derived from HDL-like particles from glial cells, the main producer of apoE in the CNS, as the apoE-containing HDL secreted by these cells differs from plasma HDL (61, 62). Since decreases or increases in ABCA1 expression alter the absolute level of apoE without affecting *Apoe* transcription, understanding how ABCA1 alters apoE metabolism in the brain will be important. Finally, while behavioral studies with APP Tg mice can be difficult to interpret, it may be useful to compare the cognitive performance over the lifespan of APP Tg mice that are *Abca1*$^{-/-}$ or overexpress ABCA1. The results of these studies could help further determine whether enhancing ABCA1 function is an attractive target for AD therapeutics.

Methods

Creation of PrP-mAbca1 Tg mice. Murine *Abca1* was cloned from RNA isolated from mouse liver using the RNeasy kit (QIAGEN). Random primer RT-PCR was performed using the First Strand cDNA Synthesis Kit (Roche Applied Sciences) to amplify 4 sections of ABCA1 cDNA that were inserted into the pcDNA3.1 vector (Invitrogen) and ligated together to make the full-length mouse *Abca1* cDNA. The correct sequence and orientation of the gene was verified by complete sequencing. *Abca1* cDNA was excised from pcDNA3.1 using XhoI and inserted into the cloning site of the MoPrP.HD-N171 TG mouse vector (63), a kind gift from David Borchelt, University of Florida, Gainesville, Florida, USA. The vector-insert boundary was sequenced to verify the proper orientation of the gene, and the Bluescript sequence was removed by Not I digestion to shorten and linearize the vector. The Mouse Genetics Core Laboratory at Washington University then produced the Tg mice using the *PrP-mAbca1* transgene.

Animals and tissue collection. All animal experiments were approved by the animal studies committee at Washington University. All animals used for in vivo experiments were either 3 or 12 months old. The founders were on a 50% C57BL/6/50% CBA genetic background and were bred to pure C57BL/6 mice. The mice used for experiments were from the F_2 or F_3 generations and were therefore approximately 12.5%–6.25% CBA, respectively, with the majority of the background being C57BL/6. To control for genetic background effects, non-Tg littermate mice were always used as controls in experiments with the *PrP-mAbca1* Tg mice from the appropriate line. *Abca1*$^{-/-}$ mice were obtained from the Jackson Laboratory.

CSF was obtained as previously described (64). For tissue collection, animals were anesthetized with pentobarbital and perfused with PBS-heparin (3 U/ml). Regional brain dissection and dissection of body tissues was performed. Tissue samples were frozen on dry ice and stored at –80°C until further analysis.

Testes studies. Testes were harvested and processed as described previously (30, 31). Briefly, the tissue was fixed either in 4% paraformaldehyde for TUNEL staining and immunohistochemistry or in Bouin fixative followed by paraffin embedding and serial sectioning (6 μM) for histological analysis. For quantification, 50 seminiferous tubules from random cross-sections of each testis were counted. An anti-GCNA1 antibody (1:200, rat polyclonal; a gift from George Enders, University of Kansas Medical Center, Kansas City, Kansas, USA) was used to identify germ cells, and an anti-GATA4 (1:200, goat polyclonal; Santa Cruz Biotechnology Inc.) antibody was used to identify Sertoli cells.

HJ1. At the time of these experiments, we found no satisfactory commercially available antibody that detected murine ABCA1 on Western blots and therefore created our own antibody. Using cDNA made from mouse liver RNA, we cloned the N-terminal extracellular loop of ABCA1 from bp 465–2,184 into the pRSET B vector (Invitrogen) using NcoI and HindII. The recombinant protein was expressed in *E. coli* and purified from inclusion bodies. The protein was then used as an immunogen for production of a monoclonal antibody according to protocols established by the Washington University School of Medicine Hybridoma Center (65).

Western blotting. Tissue was sonicated in 10 μl/mg of RIPA buffer with protease inhibitors. Total protein in the tissue homogenates was determined by micro-BCA assay (Pierce). Equal amounts of total protein from each animal were loaded into the wells of pre-made gels from Invitrogen. Total protein (10 μg) was loaded for higher-abundance proteins (e.g., apoE), and 50–80 μg of total protein was loaded for lower-abundance

proteins (e.g., LRP). After electrophoresis, protein was transferred to nitrocellulose membranes and blocked with 4% milk. The blots were probed with the following antibodies: anti-ABCA1 (HJ1, described above), anti–apoA-I (Biodesign K23001R), anti-apoE (Calbiochem 178479), anti-apoJ (Covance SIG-39080), anti-APP (Zymed 51-2700), anti-LDLR (Novus NB110-57162), anti-LRP (a generous gift from Guojun Bu, Washington University), anti-ABCG1 (Novus NB400-132), and anti-tubulin (Sigma-Aldrich T5168). The blots were then washed and incubated with the appropriate HRP-linked secondary antibody. Bands were visualized with the SuperSignal enhanced chemoluminescence agent (Pierce) and imaged with a Kodak Image Station.

ACM. Astrocytes were cultured, and ACM was fractionated as described previously (18). Briefly, cerebral lobes were dissected from 1- to 3-day-old mouse pups, and the meninges were removed. Tissue was triturated and passed through a 100-μm cell strainer. Cells were grown in 1:1 DMEM/F12 medium containing 10% FBS, 10% horse serum (HS), 10 ng/ml EGF, 1× penicillin/streptomycin, 1× Fungizone, and 1 mM sodium pyruvate. Serum-free medium contained 1× N2 supplement (Invitrogen) in place of FBS and HS. Confluent astrocytes were grown in serum-free medium for 3 days, and the conditioned medium was collected.

For fractionation of ACM, 40 ml of media was concentrated into 1 ml with a 10-kDa molecular weight cut-off concentrator (Millipore). The concentrated ACM was passed through tandem Superose-6 HR 10/30 columns (Amersham Biosciences). Cholesterol was measured as previously described (18) using the Amplex Red kit from Molecular Probes (Invitrogen). Phospholipid was measured using the Wako Phospholipids C kit. apoE protein was measured using a sensitive sandwich ELISA that has previously been described (18).

Nondenaturing gradient gel electrophoresis. Samples of ACM or CSF were mixed 1:1 with native sample buffer and electrophoresed on 4%–20% Tris-Glycine gels (Invitrogen). Proteins with known hydrated diameters were used as size standards (Amersham). Proteins were transferred to a nitrocellulose membrane, probed with a goat anti-mouse apoE antibody at 1:100 (M-20 from Santa Cruz Biotechnology Inc.), washed, and probed with horse anti-goat IgG linked to HRP at 1:1,000 (Vector Laboratories). Bands were visualized with enhanced chemoluminescence (Pierce) and imaged with a Kodak Image Station.

Measurement of apoE protein in brain and CSF. Brain tissue was subjected to a serial extraction method that has previously been used to extract different pools of Aβ (36). Tissue was homogenized in 10 μl/mg carbonate buffer (100 mM sodium, 50 mM NaCl, protease inhibitors, pH 11.5) and centrifuged at 20,000 *g* for 25 minutes. The carbonate extract was collected, and the pellet was rehomogenized in 500 μl of guanidine buffer (5 M guanidine, 50 mM Tris, protease inhibitors, pH 8.0). The guanidine homogenate was rotated for 3 hours at room temperature, then centrifuged at 20,000 *g* for 25 minutes and the guanidine extract collected. apoE in carbonate and guanidine brain extracts, as well as CSF, was measured using a previously described ELISA (18).

Real-time RT-PCR of mouse apoE. Real-time RT-PCR for mouse apoE was performed exactly as described before (18). Briefly, RNA was extracted from brain tissue using the RNeasy kit (QIAGEN). RT-PCR for mouse apoE was performed with the Brilliant SYBR Green QRT-PCR Master Mix 1-Step kit (Stratagene) and RT-PCR for 18S ribosomal RNA was performed using reagents from Applied Biosystems. The ABI Prism 7000 sequence detection system was used for running and analyzing the real-time RT-PCR. Mouse apoE mRNA was normalized to 18S ribosomal RNA.

Statistics. All analyses were performed using PRISM version 5.00 (GraphPad). Error bars represent SEM. For all tests of significance between 2 groups, either a 2-tailed Student's *t* test or a Mann-Whitney *U* test was performed. A *P* value of less than 0.05 was considered significant.

Acknowledgments

This work was partly supported by NIH grants AG13956 (to D.M. Holtzman), HD047396 (to S. Jain), the O'Brien Center for Kidney Disease Research (P30 DK079333), and Eli Lilly and Co. C.L. Wellington is supported by a salary award from the Canadian Institutes of Health Research. J. Kim is supported by an Alzheimer disease research grant, a program of the American Health Assistance Foundation (AHAF).

Received for publication August 15, 2007, and accepted in revised form November 28, 2007.

Address correspondence to: David M. Holtzman, Washington University, Department of Neurology, 660 S. Euclid Avenue, Box 8111, St. Louis, Missouri 63110, USA. Phone: (314) 362-9872; Fax: (314) 362-1771; E-mail: holtzman@neuro.wustl.edu.

Suzanne E. Wahrle and Hong Jiang contributed equally to this work.

1. Glomset, J.A. 1968. The plasma lecithins:cholesterol acyltransferase reaction. *J. Lipid Res.* **9**:155–167.
2. Van Eck, M., Pennings, M., Hoekstra, M., Out, R., and Van Berkel, T.J. 2005. Scavenger receptor BI and ATP-binding cassette transporter A1 in reverse cholesterol transport and atherosclerosis. *Curr. Opin. Lipidol.* **16**:307–315.
3. Lee, J.Y., and Parks, J.S. 2005. ATP-binding cassette transporter AI and its role in HDL formation. *Curr. Opin. Lipidol.* **16**:19–25.
4. Brewer, H.B., Jr., Remaley, A.T., Neufeld, E.B., Basso, F., and Joyce, C. 2004. Regulation of plasma high-density lipoprotein levels by the ABCA1 transporter and the emerging role of high-density lipoprotein in the treatment of cardiovascular disease. *Arterioscler. Thromb. Vasc. Biol.* **24**:1755–1760.
5. Wang, X., et al. 2007. Macrophage ABCA1 and ABCG1, but not SR-BI, promote macrophage reverse cholesterol transport in vivo. *J Clin. Invest.* **117**:2216–2224.
6. Brooks-Wilson, A., et al. 1999. Mutations in ABC1 in Tangier disease and familial high-density lipoprotein deficiency. *Nat. Genet.* **22**:336–345.
7. Bodzioch, M., et al. 1999. The gene encoding ATP-binding cassette transporter 1 is mutated in Tangier disease. *Nat. Genet.* **22**:347–351.
8. Rust, S., et al. 1999. Tangier disease is caused by mutations in the gene encoding ATP-binding cassette transporter 1. *Nat. Genet.* **22**:352–355.
9. Remaley, A.T., et al. 1999. Human ATP-binding cassette transporter 1 (ABC1): genomic organization and identification of the genetic defect in the original Tangier disease kindred. *Proc. Natl. Acad. Sci. U. S. A.* **96**:12685–12690.
10. Mott, S., et al. 2000. Decreased cellular cholesterol efflux is a common cause of familial hypoalphalipoproteinemia: role of the ABCA1 gene mutations. *Atherosclerosis.* **152**:457–468.
11. Lawn, R.M., et al. 1999. The Tangier disease gene product ABC1 controls the cellular apolipoprotein-mediated lipid removal pathway. *J. Clin. Invest.* **104**:R25–R31.
12. Brousseau, M.E., et al. 2000. Cellular cholesterol efflux in heterozygotes for tangier disease is markedly reduced and correlates with high density lipoprotein cholesterol concentration and particle size. *J. Lipid Res.* **41**:1125–1135.
13. Schaefer, E.J., et al. 1981. Metabolism of high density lipoprotein subfractions and constituents in Tangier disease following the infusion of high density lipoproteins. *J. Lipid Res.* **22**:217–228.
14. Schaefer, E.J., et al. 1978. Metabolism of high-density lipoprotein apolipoproteins in Tangier disease. *N. Engl. J. Med.* **299**:905–910.
15. Joyce, C.W., et al. 2002. The ATP binding cassette transporter A1 (ABCA1) modulates the development of aortic atherosclerosis in C57BL/6 and apoE-knockout mice. *Proc. Natl. Acad. Sci. U. S. A.* **99**:407–412.
16. Singaraja, R.R., et al. 2002. Increased ABCA1 activity protects against atherosclerosis. *J. Clin. Invest.* **110**:35–42.
17. Van Eck, M., et al. 2006. Macrophage ATP-binding cassette transporter A1 overexpression inhibits atherosclerotic lesion progression in low-density lipoprotein receptor knockout mice. *Arterioscler. Thromb. Vasc. Biol.* **26**:929–934.
18. Wahrle, S.E., et al. 2004. ABCA1 is required for normal central nervous system ApoE levels and for lipidation of astrocyte-secreted apoE. *J. Biol. Chem.* **279**:40987–40993.
19. Hirsch-Reinshagen, V., et al. 2004. Deficiency of ABCA1 impairs apolipoprotein E metabolism in brain. *J. Biol. Chem.* **279**:41197–41207.
20. Koldamova, R., Staufenbiel, M., and Lefterov, I. 2005. Lack of ABCA1 considerably decreases brain ApoE level and increases amyloid deposition in APP23 mice. *J. Biol. Chem.* **280**:43224–43235.

21. Wahrle, S.E., and Holtzman, D.M. 2007. Apolipoprotein E, amyloid beta-peptide and Alzheimer's disease. In *Neurobiology of Alzheimer's disease*. D. Dawbarn and S.J. Allen, editors. Oxford University Press. Oxford, United Kingdom. 161–172.
22. Spires, T.L., et al. 2005. Dendritic spine abnormalities in amyloid precursor protein transgenic mice demonstrated by gene transfer and intravital multiphoton microscopy. *J. Neurosci.* **25**:7278–7287.
23. Wahrle, S.E., et al. 2005. Deletion of Abca1 increases Abeta deposition in the PDAPP transgenic mouse model of Alzheimer disease. *J. Biol. Chem.* **280**:43236–43242.
24. Hirsch-Reinshagen, V., et al. 2005. The absence of ABCA1 decreases soluble ApoE levels but does not diminish amyloid deposition in two murine models of Alzheimer disease. *J. Biol. Chem.* **280**:43243–43256.
25. Singaraja, R.R., et al. 2001. Human ABCA1 BAC transgenic mice show increased high density lipoprotein cholesterol and ApoAI-dependent efflux stimulated by an internal promoter containing liver X receptor response elements in intron 1. *J. Biol. Chem.* **276**:33969–33979.
26. Hirsch-Reinshagen, V., et al. 2007. Physiologically regulated transgenic ABCA1 does not reduce amyloid burden or amyloid-beta peptide levels in vivo. *J. Lipid Res.* **48**:914–923.
27. Vaisman, B.L., et al. 2001. ABCA1 overexpression leads to hyperalphalipoproteinemia and increased biliary cholesterol excretion in transgenic mice. *J. Clin. Invest.* **108**:303–309.
28. Selva, D.M., et al. 2004. The ATP-binding cassette transporter 1 mediates lipid efflux from Sertoli cells and influences male fertility. *J. Lipid Res.* **45**:1040–1050.
29. Cavelier, L.B., et al. 2001. Regulation and activity of the human ABCA1 gene in transgenic mice. *J. Biol. Chem.* **276**:18046–18051.
30. Jain, S., et al. 2004. Mice expressing a dominant-negative Ret mutation phenocopy human Hirschsprung disease and delineate a direct role of Ret in spermatogenesis. *Development.* **131**:5503–5513.
31. Naughton, C.K., Jain, S., Strickland, A.M., Gupta, A., and Milbrandt, J. 2006. Glial cell-line derived neurotrophic factor-mediated RET signaling regulates spermatogonial stem cell fate. *Biol. Reprod.* **74**:314–321.
32. Bales, K.R., et al. 1999. Apolipoprotein E is essential for amyloid deposition in the APP(V717F) transgenic mouse model of Alzheimer's disease. *Proc. Natl. Acad. Sci. U. S. A.* **96**:15233–15238.
33. Bales, K.R., et al. 1997. Lack of apolipoprotein E dramatically reduces amyloid beta-peptide deposition. *Nat. Genet.* **17**:263–264.
34. Holtzman, D.M., et al. 2000. Apolipoprotein E isoform-dependent amyloid deposition and neuritic degeneration in a mouse model of Alzheimer's disease. *Proc. Natl. Acad. Sci. U. S. A.* **97**:2892–2897.
35. Games, D., et al. 1995. Alzheimer-type neuropathology in transgenic mice overexpressing V717F beta-amyloid precursor protein. *Nature.* **373**:523–527.
36. DeMattos, R.B., et al. 2004. ApoE and clusterin cooperatively suppress abeta levels and deposition. Evidence that ApoE regulates extracellular abeta metabolism in vivo. *Neuron.* **41**:193–202.
37. Irizarry, M.C., et al. 2000. Apolipoprotein E affects the amount, form, and anatomical distribution of amyloid beta-peptide deposition in homozygous APP(V717F) transgenic mice. *Acta Neuropathol. (Berl.)* **100**:451–458.
38. Strittmatter, W.J., et al. 1993. Apolipoprotein E: high-avidity binding to beta-amyloid and increased frequency of type 4 allele in late-onset familial Alzheimer disease. *Proc. Natl. Acad. Sci. U. S. A.* **90**:1977–1981.
39. Schmechel, D.E., et al. 1993. Increased amyloid beta-peptide deposition in cerebral cortex as a consequence of apolipoprotein E genotype in late-onset Alzheimer disease. *Proc. Natl. Acad. Sci. U. S. A.* **90**:9649–9653.
40. Greenberg, S.M., Rebeck, G.W., Vonsattel, J.P., Gomez-Isla, T., and Hyman, B.T. 1995. Apolipoprotein E epsilon 4 and cerebral hemorrhage associated with amyloid angiopathy. *Ann. Neurol.* **38**:254–259.
41. Corder, E.H., et al. 1993. Gene dose of apolipoprotein E type 4 allele and the risk of Alzheimer's disease in late onset families. *Science.* **261**:921–923.
42. Strittmatter, W.J., et al. 1993. Binding of human apolipoprotein E to synthetic amyloid beta peptide: isoform-specific effects and implications for late-onset Alzheimer disease. *Proc. Natl. Acad. Sci. U. S. A.* **90**:8098–8102.
43. Holtzman, D.M., et al. 2000. Apolipoprotein E facilitates neuritic and cerebrovascular plaque formation in an Alzheimer's disease model. *Ann. Neurol.* **47**:739–747.
44. Fryer, J.D., et al. 2003. Apolipoprotein E markedly facilitates age-dependent cerebral amyloid angiopathy and spontaneous hemorrhage in amyloid precursor protein transgenic mice. *J. Neurosci.* **23**:7889–7896.
45. Holtzman, D.M., et al. 1999. Expression of human apolipoprotein E reduces amyloid-beta deposition in a mouse model of Alzheimer's disease. *J. Clin. Invest.* **103**:R15–R21.
46. Vassar, R., et al. 1999. Beta-secretase cleavage of Alzheimer's amyloid precursor protein by the transmembrane aspartic protease BACE. *Science.* **286**:735–741.
47. Leissring, M.A., et al. 2003. Enhanced proteolysis of beta-amyloid in APP transgenic mice prevents plaque formation, secondary pathology, and premature death. *Neuron.* **40**:1087–1093.
48. DeMattos, R.B., et al. 2002. Clusterin promotes amyloid plaque formation and is critical for neuritic toxicity in a mouse model of Alzheimer's disease. *Proc. Natl. Acad. Sci. U. S. A.* **99**:10843–10848.
49. Bell, R.D., et al. 2007. Transport pathways for clearance of human Alzheimer's amyloid beta-peptide and apolipoproteins E and J in the mouse central nervous system. *J. Cereb. Blood Flow Metab.* **27**:909–918.
50. Koldamova, R., and Lefterov, I. 2007. Role of LXR and ABCA1 in the pathogenesis of Alzheimer's disease — implications for a new therapeutic approach. *Curr. Alzheimer Res.* **4**:171–178.
51. Cao, G., Bales, K.R., DeMattos, R.B., and Paul, S.M. 2007. Liver X receptor-mediated gene regulation and cholesterol homeostasis in brain: relevance to Alzheimer's disease therapeutics. *Curr. Alzheimer Res.* **4**:179–184.
52. Liang, Y., et al. 2004. A liver X receptor and retinoid X receptor heterodimer mediates apolipoprotein E expression, secretion and cholesterol homeostasis in astrocytes. *J. Neurochem.* **88**:623–634.
53. Sun, Y., Yao, J., Kim, T.W., and Tall, A.R. 2003. Expression of liver X receptor target genes decreases cellular amyloid beta peptide secretion. *J. Biol. Chem.* **278**:27688–27694.
54. Fukumoto, H., Deng, A., Irizarry, M.C., Fitzgerald, M.L., and Rebeck, G.W. 2002. Induction of the cholesterol transporter ABCA1 in central nervous system cells by liver X receptor agonists increases secreted Abeta levels. *J. Biol. Chem.* **277**:48508–48513.
55. Koldamova, R.P., et al. 2003. 22R-hydroxycholesterol and 9-cis-retinoic acid induce ATP-binding cassette transporter A1 expression and cholesterol efflux in brain cells and decrease amyloid beta secretion. *J. Biol. Chem.* **278**:13244–13256.
56. Zelcer, N., et al. 2007. Attenuation of neuroinflammation and Alzheimer's disease pathology by liver x receptors. *Proc. Natl. Acad. Sci. U. S. A.* **104**:10601–10606.
57. Burns, M.P., et al. 2006. The effects of ABCA1 on cholesterol efflux and Abeta levels in vitro and in vivo. *J. Neurochem.* **98**:792–800.
58. LaDu, M.J., et al. 1994. Isoform-specific binding of apolipoprotein E to beta-amyloid. *J. Biol. Chem.* **269**:23403–23406.
59. LaDu, M.J., et al. 1995. Purification of apolipoprotein E attenuates isoform-specific binding to beta-amyloid. *J. Biol. Chem.* **270**:9039–9042.
60. Tokuda, T., et al. 2000. Lipidation of apolipoprotein E influences its isoform-specific interaction with Alzheimer's amyloid beta peptides. *Biochem. J.* **348**:359–365.
61. LaDu, M.J., et al. 1998. Nascent astrocyte particles differ from lipoproteins in CSF. *J. Neurochem.* **70**:2070–2081.
62. Fagan, A.M., et al. 1999. Unique lipoproteins secreted by primary astrocytes from wild type, apoE (–/–), and human apoE transgenic mice. *J. Biol. Chem.* **274**:30001–30007.
63. Borchelt, D.R., et al. 1996. A vector for expressing foreign genes in the brains and hearts of transgenic mice. *Genet. Anal.* **13**:159–163.
64. DeMattos, R.B., et al. 2002. Plaque-associated disruption of CSF and plasma amyloid-beta (Abeta) equilibrium in a mouse model of Alzheimer's disease. *J. Neurochem.* **81**:229–236.
65. Washington University Hybridoma Center protocols. 2007. http://pathology.wustl.edu/research/hybridoma.php.